

The Electronic Properties of a 2D Ruddlesden-Popper Perovskite and its Energy Level Alignment with a 3D Perovskite Enable Interfacial Energy Transfer

Dongguen Shin, Fengshuo Zu, Edgar R. Nandayapa, Lennart Frohloff, Emily Albert, Emil J. W. List-Kratochvil, and Norbert Koch*

The success of using 2D Ruddlesden-Popper metal halide perovskites (MHPs) in optoelectronic devices has ignited great interest as means for energy level tuning at the interface with 3D MHPs. Inter alia, the application of 2D phenylethylammonium lead quaternary iodide (PEA₂PbI₄)/3D MHPs interfaces has improved various optoelectronic devices, where a staggered type-II energy level alignment is often assumed. However, a type-II heterojunction seems to contradict the enhanced photoluminescence observed for 2D PEA₂PbI₄/3D MHP interfaces, which raises fundamental questions about the electronic properties of such junctions. In this study, using direct and inverse photoelectron spectroscopy, it is revealed that a straddling type-I energy level alignment is present at 2D PEA₂PbI₄/3D methylammonium lead triiodide (MAPbI₃) interfaces, thus explaining that the photoluminescence enhancement of the 3D perovskite is induced by energy transfer from the 2D perovskite. These results provide a reliable fundamental understanding of the electronic properties at the investigated 2D/3D MHP interfaces and suggest careful (re)consideration of the electronic properties of other 2D/3D MHP heterostructures.

1. Introduction

The superior optoelectronic properties of metal halide perovskites (MHPs) have enabled notable success for their

D. Shin, F. Zu, L. Frohloff, E. Albert, E. J. W. List-Kratochvil, N. Koch
Institut für Physik & IRIS Adlershof
Humboldt-Universität zu Berlin
12489 Berlin, Germany
E-mail: norbert.koch@physik.hu-berlin.de

E. R. Nandayapa, E. J. W. List-Kratochvil, N. Koch
Helmholtz-Zentrum Berlin für Materialien und Energie GmbH
14109 Berlin, Germany

E. J. W. List-Kratochvil
Institut für Chemie
Humboldt-Universität zu Berlin
12489 Berlin, Germany

 The ORCID identification number(s) for the author(s) of this article can be found under <https://doi.org/10.1002/adfm.202208980>.

© 2022 The Authors. Advanced Functional Materials published by Wiley-VCH GmbH. This is an open access article under the terms of the Creative Commons Attribution License, which permits use, distribution and reproduction in any medium, provided the original work is properly cited.

DOI: 10.1002/adfm.202208980

application in optoelectronic devices,^[1–4] particularly remarkable in photovoltaics. However, MHPs still suffer from stability issues and the performance of MHP-based solar cells is still largely limited by significant nonradiative recombination loss in the device.^[5,6] One strategy to overcome these issues involves the use of 2D Ruddlesden-Popper (RDP) type MHPs. Due to their outstanding moisture stability and the unique quantum confinement effect,^[7–9] 2D MHPs have been recently employed in combination with 3D MHPs to enhance the performance of solar cells. The use of 2D/3D MHP heterojunctions in optoelectronic devices has led to improved efficiency and stability,^[2,3,18,19,10–17] demonstrating the possibility of further tuning the optoelectronic properties of MHP materials toward the development of further applications.

Notwithstanding the great success of the application of the 2D MHPs in both solar cells and light-emitting diodes, a fundamental understanding of their electronic properties, which is the key to further knowledge-based device optimization, is still lacking.^[20] For instance, the alignment of energy levels at 2D/3D MHP-based heterojunctions, i.e., whether it belongs to the straddling type-I or the staggered type-II situation, is still under debate. The formation of type-II junctions has generally been assumed for various 2D/3D MHP interfaces and was used for reasoning the device performance improvement.^[21–27] For instance, by assuming a constant vacuum level (or electrostatic potential) across the interface, a type-II junction was suggested for phenylethylammonium lead quaternary iodide (PEA₂PbI₄)/methylammonium lead triiodide (MAPbI₃) interfaces, as deduced from separately determined ionization energy (IE) and electron affinity (EA) values of the individual materials.^[24,28–32] However, one should be aware that the energy level alignment at an interface may be (far) off from the assumed level diagram due to compositional and structural variations compared to an individual material surface.^[33,34] On the other hand, an improvement of the photoluminescence (PL) quantum yield of 3D MHPs were observed upon constructing 2D/3D MHP junctions. Although such PL enhancement was attributed to a suppression of nonradiative

recombination by introducing the 2D perovskite at the surface of the 3D MHP, the possibility of the presence of a type-I junction cannot be readily ruled out, because a significant loss in PL yield is expected for a type-II junction due to interfacial charge transfer.^[15,21,22,25,26,35–38] It is noted that an energy level alignment at the border of type-II and type-I was reported for 2D/3D interfaces, deduced from UV photoelectron spectroscopy (UPS) depth profiling measurements employing gas-cluster ion sputtering.^[22] While the incremental removal of material by sputtering with cluster ions is more gentle than sputtering with conventional atomic ions, it is still challenging to explore the original energy level at the unperturbed interface, because composition changes induced by the depth profiling process cannot be readily excluded, which could influence the electronic structure. It has been acknowledged in this context that the energy levels of 3D MHP films can undergo drastic changes depending on the stoichiometry, the substrate work function,^[39–43] and sample preparation/handling conditions.^[39,40,44] Therefore, thorough and systematic investigations of the electronic properties of 2D MHPs and their interfaces are still highly desirable.

In this work, the intrinsic electronic properties of the prototypical PEA_2PbI_4 2D perovskite, to the best of our knowledge for the first time, were investigated by combining UPS and inverse photoelectron spectroscopy (IPES), from which a fundamental bandgap of 2.65 eV was determined. The dependence of the electronic properties of 2D PEA_2PbI_4 and its interface with 3D MAPbI_3 as a function of substrate work function (Φ_{sub}) was also explored. We find that PEA_2PbI_4 perovskite films exhibit slight n-type character with nearly constant Fermi level (E_{F}) position in the energy gap, independent of Φ_{sub} . In contrast, the E_{F} position for $\text{PEA}_2\text{PbI}_4/\text{MAPbI}_3$ junctions significantly changes from seemingly n-type to p-type character by as much as ≈ 0.74 eV upon varying Φ_{sub} . With further photoemission and photoluminescence data, we confirm that the $\text{PEA}_2\text{PbI}_4/\text{MAPbI}_3$ interface is a type-I heterojunction and that the enhanced PL yield of the 3D perovskite interfaced with the 2D perovskite is caused by interfacial energy transfer.

2. Results and Discussion

2.1. Fundamental Electronic Properties of the 2D PEA_2PbI_4 Perovskite

We start by studying the intrinsic electronic properties of 2D PEA_2PbI_4 perovskite films by means of UPS and IPES. A ≈ 200 nm thick PEA_2PbI_4 film deposited on a substrate comprised of indium-tin-oxide (ITO) covered with a thin layer of polyethyleneimine (PEIE) [substrate work function (Φ_{PEIE}) of 3.85 eV] exhibits work function of 4.5 eV, as derived from the secondary electron cutoff (SECO) region shown in **Figure 1a**. The valence and conduction band onset values of PEA_2PbI_4 film are determined to be 1.73 eV and -0.92 eV (binding energy with respect to E_{F} at 0 eV), respectively, from which a fundamental bandgap (E_{g}) of 2.65 eV is directly determined. Given the optical gap (E_{opt}) of 2.36 eV, obtained from both a Tauc plot of the absorption spectrum and PL measurements (Figure S1 in the Supporting Information), an exciton binding energy ($E_{\text{b,exc}}$) of ≈ 290 meV is obtained, which agrees well with previously derived values.^[9,45] Thus, the fundamental bandgap should be considered in order to accurately establish the band alignment at PEA_2PbI_4 -related interfaces, instead of the optical gap. At this point, although E_{F} for PEA_2PbI_4 is not mid-gap but located closer to the conduction band minimum (CBM), it is not yet conclusive whether PEA_2PbI_4 is an n-type semiconductor, because the apparent electrical character of perovskites can change drastically upon varying the substrate.^[39,40] In order to get a full picture of PEA_2PbI_4 films' electronic properties, the dependence of E_{F} on the substrate work function was further investigated.

To that end, ≈ 200 nm thick PEA_2PbI_4 films were deposited on various substrates with Φ_{sub} ranging from 3.57 eV to 5 eV (see Figure S2 in Supporting Information for details of the substrate work function). As seen in **Figure 2a**, Φ and VB onset of PEA_2PbI_4 films exhibit almost constant values at ≈ 4.53 eV and 1.65 eV, respectively, regardless of Φ_{sub} . The fixed E_{F} position in the energy gap can be due to two underlying mechanisms: i) the presence of a significant gap density of states of the

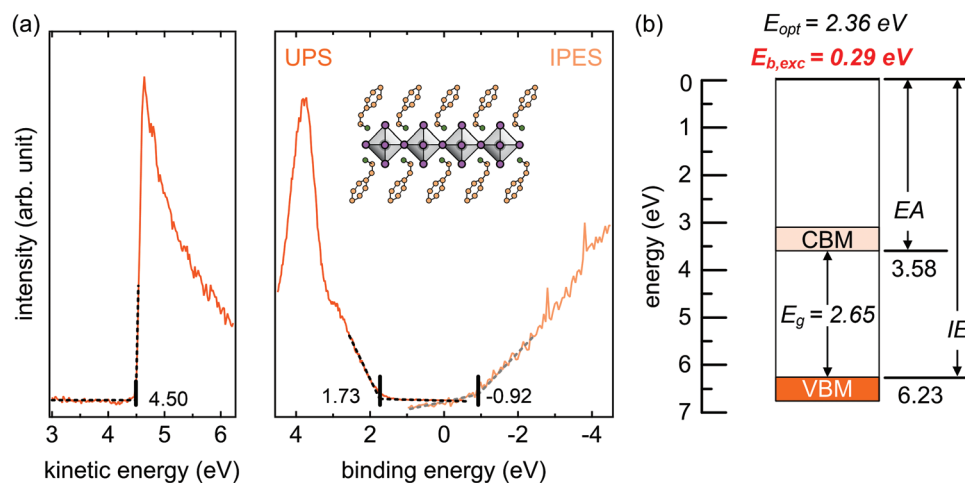


Figure 1. a) UPS and IPES spectra of a 200 nm thick PEA_2PbI_4 film on a PEIE/ITO substrate. b) Energy levels of PEA_2PbI_4 extracted from the UPS and IPES data. The inset in panel (a) represents the structure of PEA_2PbI_4 .

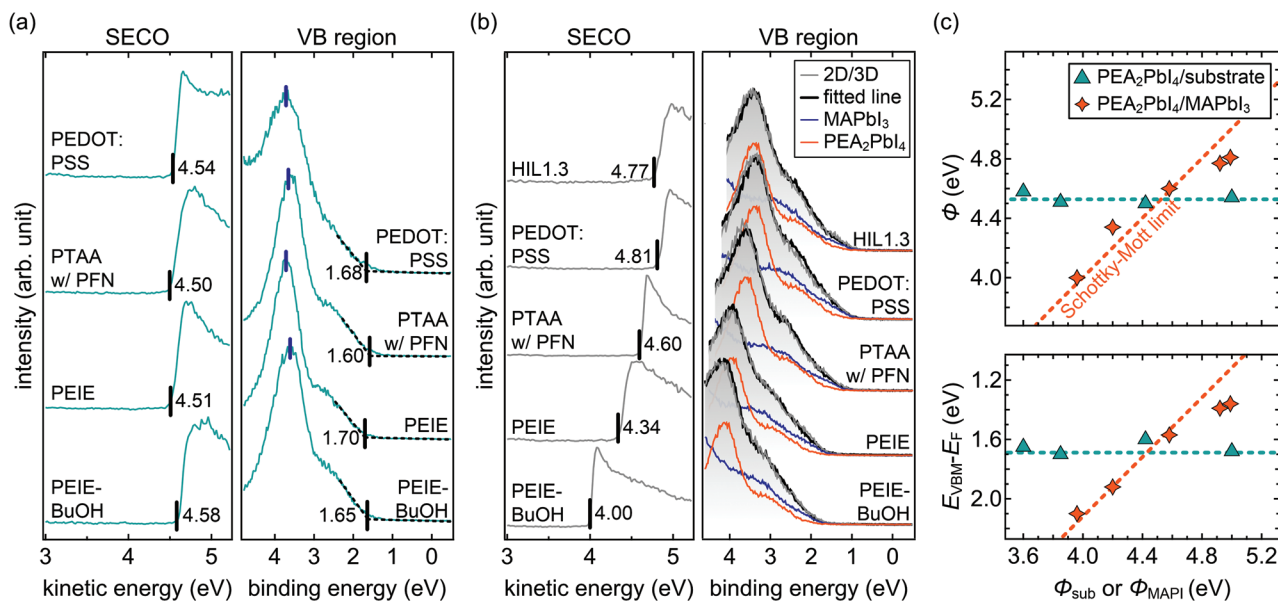


Figure 2. UPS spectra of a) ≈ 200 nm thick PEA_2PbI_4 films and b) $\text{PEA}_2\text{PbI}_4/\text{MAPbI}_3$ (2D/3D) heterostructures on various substrates. c) Work function (Φ) and valence band maxima (VBM, $E_{\text{VBM}}-E_{\text{F}}$) values derived from UPS spectra of PEA_2PbI_4 films and $\text{PEA}_2\text{PbI}_4/\text{MAPbI}_3$ heterostructures as a function of the substrate work function (Φ_{sub}).

semiconductor that pins E_{F} at a certain position in the energy gap; [46] ii) the occurrence of “intrinsic” E_{F} -pinning (for a semiconductor without surface or gap states) in contact with Φ_{sub} close to or beyond the IE (or EA) of the semiconductor. This situation results in interfacial charge transfer to establish electronic equilibrium and subsequent E_{F} -pinning at the respective band edges at the interface.^[34,47,48] We do not observe a notable gap state density on the surface of the PEA_2PbI_4 films, thus the E_{F} position at the surface measured by UPS is expected to also represent its position in the bulk. Moreover, the presence of gap states in PEA_2PbI_4 would lead to a broad PL emission near 1.7 eV (mostly due to iodine vacancies),^[49,50] which was not observed in our experiments (see Figure S1, Supporting Information). Thus, the change of the vacuum level (or electrostatic potential) between the substrate and PEA_2PbI_4 can then be attributed to the formation of an interface dipole or band bending, where in the latter case the space-charge region would be expected to be much shorter than the PEA_2PbI_4 film thickness of ≈ 200 nm. This already indicates that the energy levels probed at the surface can differ significantly from those at the buried interface, in case the depletion width is shorter than the actual film thickness.^[51] These findings for the 2D perovskite are in strong contrast to the case of the 3D MAPbI_3 , which behaves like an intrinsic semiconductor, with a largely tunable E_{F} position within the band gap by up to 0.78 eV upon varying the substrates’ work function. (Figure S3, Supporting Information).^[40]

To confirm the bulk n-type character of PEA_2PbI_4 and to obtain insights into the 2D/3D perovskite interfaces, similar experiments using various Φ_{sub} were performed for $\text{PEA}_2\text{PbI}_4/\text{MAPbI}_3$ heterostructures, where the 2D layer deposited on top of the 3D material was kept intentionally very thin (approximately monolayer regime) to exclude band bending effects within the 2D perovskite. As displayed in Figure 2b, upon

increasing Φ_{sub} from 3.57 eV to 5.70 eV, the heterostructure Φ also increases from 4.00 eV to 4.77 eV. The valence region exhibits similar shifts toward lower binding energy, however, its appearance resembles a superposition of PEA_2PbI_4 and MAPbI_3 features. To determine the band edges at the $\text{PEA}_2\text{PbI}_4/\text{MAPbI}_3$ junctions, the valence band spectra are thus fitted with contributions from pristine PEA_2PbI_4 as well as pristine MAPbI_3 , as presented in Figure 2b (right panel). We would like to mention that the determination of the valence band onset values for 3D perovskites is done on a logarithmic intensity scale in order to accurately infer the topmost band edge.^[41,52,53] In contrast, the band edges for 2D MHPs can be directly obtained by extrapolating the photoelectron intensity on a linear intensity scale toward the background because of their non-dispersive top valence bands,^[54,55] similar to what is conventional for organic semiconductors.^[56,57] The observation of valence features of MAPbI_3 in the heterostructure spectra indicates indeed a sub-monolayer coverage of PEA_2PbI_4 on the surface, given the very surface sensitive nature of UPS with an electron inelastic mean free path of $\approx 1\text{--}2$ nm.^[58] Upon increasing the thickness of the PEA_2PbI_4 layer on top of MAPbI_3 (Figure S4, Supporting Information), the valence band spectra are found to be composed of PEA_2PbI_4 features only, accompanied by a shift toward the energy positions found for the thick PEA_2PbI_4 films on other substrates (Figure 2a), indicating a build-up of a space-charge region. It is noted that the presence of a thick 2D PEA_2PbI_4 layer on top of MAPbI_3 was confirmed by comparing the valence band structure of the 2D PEA_2PbI_4 and thick $\text{PEA}_2\text{PbI}_4/\text{MAPbI}_3$ films with PEA_2PbI_4 single crystal, as shown in Figure S5 (Supporting Information). A nearly identical lineshape in the valence region is observed for the PEA_2PbI_4 films and single crystals; in addition, XPS measurements on $\text{PEA}_2\text{PbI}_4/\text{MAPbI}_3$ and PEA_2PbI_4 films both reveal the atomic ratio of I/Pb and I/N to be ≈ 4.0 and 1.8, respectively, in full

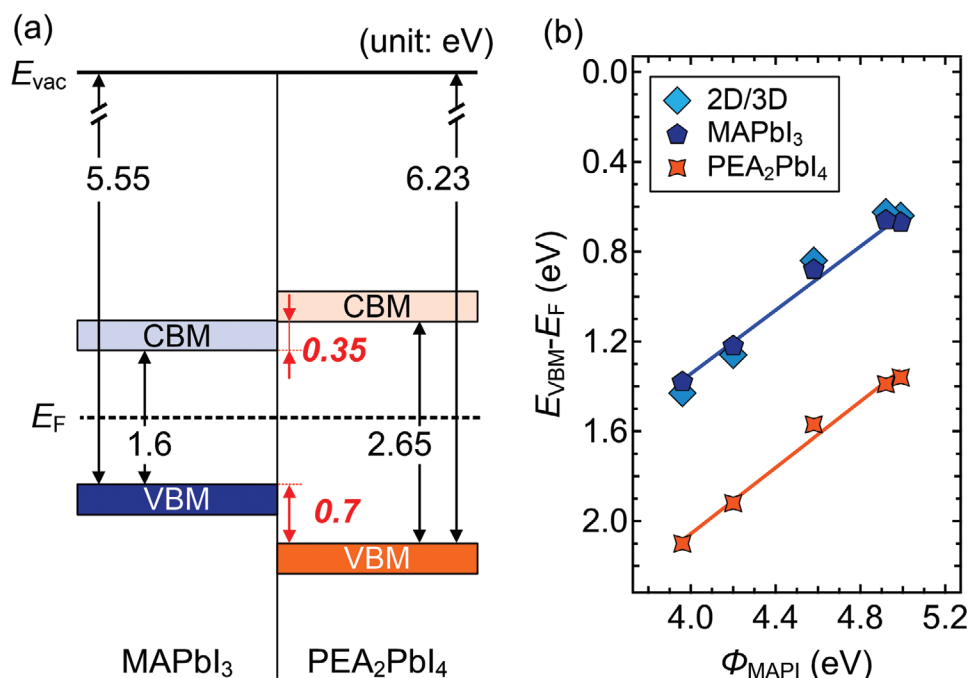


Figure 3. a) Energy level diagram of the PEA₂PbI₄/MAPbI₃ heterostructure. b) Valence band maxima ($E_{\text{VBM}}-E_{\text{F}}$) of 2D/3D stack, MAPbI₃ films (thickness of ≈ 500 nm), and PEA₂PbI₄ films (sub-monolayer). The VBM of 2D/3D stack was extracted by fitting the spectra with the contributions from MAPbI₃ and PEA₂PbI₄.

agreement with the 2D PEA₂PbI₄ stoichiometry (Figures S5 and S6, Supporting Information).

The results obtained from the UPS measurements are summarized in Figure 2c. It can be clearly seen that for the thick PEA₂PbI₄ films of ≈ 200 nm, the E_{F} position is “pinned” in the energy gap on the surface regardless of Φ_{sub} . On the other hand, for the thin (sub-monolayer) PEA₂PbI₄ films on the MAPbI₃ substrates, Φ increases linearly upon increasing Φ_{sub} with a slope ($= \frac{d\Phi}{d\Phi_{\text{sub}}}$) close to unity, indicating a vacuum-level alignment situation at the 2D/3D interface. Thus, the above observations rule out the presence of a significant gap density of states at the interface, as otherwise a fixed E_{F} position would also be expected for the PEA₂PbI₄/MAPbI₃ heterostructures.

The energy level alignment at PEA₂PbI₄/MAPbI₃ interface is then summarized in Figure 3a. This clearly confirms the formation of type-I heterojunction at the PEA₂PbI₄/MAPbI₃ interface directly from photoemission data, which yields energy offsets of ≈ 0.35 eV and ≈ 0.70 eV for electron and hole extraction, respectively. We note that the ultrathin PEA₂PbI₄ layer in our heterojunction might experience strain at the interface with the 3D perovskite, which was reported to affect the bandgap of perovskites.^[59] We investigated to what extent the bandgap of the thin PEA₂PbI₄ layer differs from a thick (200 nm) film by photoluminescence measurements, as shown in Figure S7 (Supporting Information). We observe that the PL peak of the 2D PEA₂PbI₄ layer in the 2D/3D perovskite film exhibits a comparably small shift of 13 meV as compared to that of the 200 nm PEA₂PbI₄ film. This energy shift is indeed likely caused by the presence of strain at the 2D/3D interface owing to the relaxation of the PEA cation toward the interface. However, the observed

small bandgap shift of 2D PEA₂PbI₄ in the 2D/3D perovskite junction does not impact our key finding of the type-I energy level alignment at the interface. Notably, the level alignment at the interfaces, i.e., the energy offsets for charge extraction, is found to be independent of the underlying MAPbI₃ work function (and the used Φ_{sub}), as illustrated in Figure 3b. In contrast to the type-II alignment, as often assumed in the community for the PEA₂PbI₄/MAPbI₃ interface, the type-I junction identified here does not favor efficient charge transfer from the 3D perovskite to the PEA₂PbI₄ layer. Consequently, the effect of PL enhancement of the 3D perovskite upon contact formation with a 2D PEA₂PbI₄ layer is more likely rooted in interfacial energy transfer as opposed to the widely suggested passivation effect.^[3,15,23,28]

To demonstrate efficient energy transfer at our 2D/3D interface, we first compare the steady-state PL spectra of MAPbI₃ with and without the sub-monolayer PEA₂PbI₄ layer on top in a vacuum environment (base pressure of 10^{-3} mbar), where photoexcitation at 3.06 eV and 1.90 eV was applied, respectively. From both, the absorption and PL spectra of thick PEA₂PbI₄ films, as shown in Figure S1 (Supporting Information), an optical transition at 2.36 eV is observed, which overlaps with the absorption of MAPbI₃. Such spectral overlap between the PL of the PEA₂PbI₄ and the absorption of the MAPbI₃ implies the possibility of Förster-type resonance energy transfer (FRET) across the interface,^[60–62] and can result in the enhancement of the PL emission of MAPbI₃. This is unambiguously inferred from Figure 4a, where a strong PL enhancement of MAPbI₃ is observed (centered at 1.60 eV) upon the addition of a PEA₂PbI₄ when excited at 3.06 eV. In contrast, the PL intensity of MAPbI₃ remains unchanged upon excitation at 1.90 eV, which can only

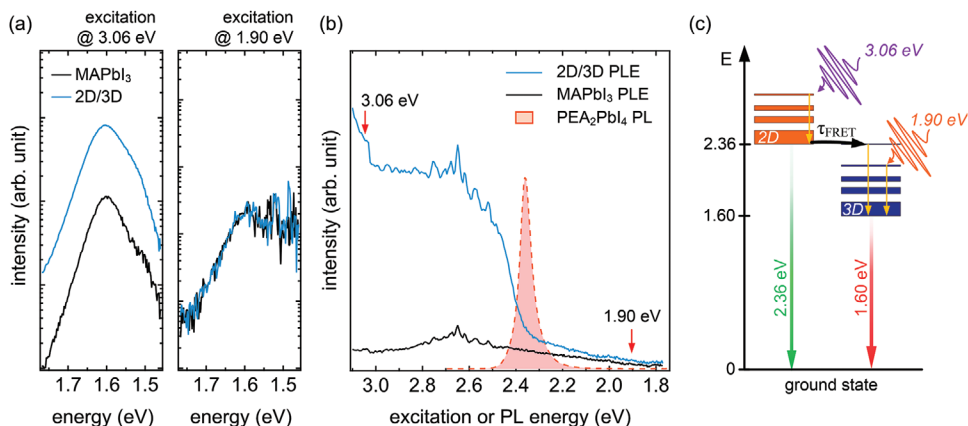


Figure 4. a) Steady-state PL spectra of MAPbI₃ and 2D/3D films on quartz substrates with excitation energy of (left) 3.06 eV and (right) 1.90 eV. b) Photoluminescence excitation (PLE) spectra of MAPbI₃ and 2D/3D films monitored at 1.60 eV (i.e., optical gap of MAPbI₃) and PL spectra of PEA₂PbI₄ on quartz substrates c) Schematic energy level diagram showing PL and energy transfer processes at the 2D/3D perovskites interface.

excite MAPbI₃. Moreover, excitation energy-dependent photoluminescence (photoluminescence excitation, PLE) measurements are conducted, which allow for tracking the PL intensity at the emission of MAPbI₃ (1.60 eV) upon varying the excitation energy, as shown in Figure 4b. We observed for both 2D/3D perovskite and 3D MAPbI₃ films a gradual increase of PL intensity upon increasing excitation energy occurs. However, a significant PL enhancement at and beyond excitation energy of ≈ 2.36 eV is observed for the 2D/3D perovskite film, which in contrast is absent for the pure 3D MAPbI₃ sample. The sharp PL enhancement for the 2D/3D perovskite film at 2.36 eV strongly overlaps with the PL emission of the 2D PEA₂PbI₄ perovskite and thus provides solid evidence for the energy transfer process at the 2D/3D interface.

These observations clearly rule out passivation as the cause of the PL enhancement at the PEA₂PbI₄/MAPbI₃ junction, and FRET could well account for the improvement.

To further corroborate these findings, time-resolved PL measurements were performed on these samples. As shown in Figure S8 (Supporting Information), by monitoring the PL decay at 1.60 eV, the information on the charge carrier lifetime of MAPbI₃ can be obtained. The time-resolved PL data show an increased carrier lifetime of MAPbI₃ upon the addition of a 2D sub-monolayer PEA₂PbI₄ on the surface. Thus, the enhanced carrier lifetime further supports the energy transfer process from 2D PEA₂PbI₄ to 3D MAPbI₃, in agreement with the formation of a type-I junction.

3. Conclusion

We investigated the electronic properties of 2D PEA₂PbI₄ films and their interfaces with the 3D MAPbI₃ perovskite by means of UPS and IPES. By employing various substrates with the work function ranging from 3.57 eV to 5.70 eV, we revealed a slight n-type character in the bulk of PEA₂PbI₄ films, where the E_F position was found to be independent of Φ_{sub} . In contrast, the formation of sub-monolayer PEA₂PbI₄ films on MAPbI₃ films demonstrated a highly tunable E_F position in the energy gap by as much as 0.81 eV, in parallel with shifts of E_F in the MAPbI₃

energy gap upon varying Φ_{sub} . This difference is rationalized by the formation of a space-charge region within PEA₂PbI₄ close to the substrate, implying that the depletion width is much shorter than the PEA₂PbI₄ film thickness of ≈ 200 nm. Thus, the probed E_F position on the surface of the thick PEA₂PbI₄ films by UPS is expected to represent its bulk electrical properties. Our photoemission data further confirm the formation of a type-I level alignment at the PEA₂PbI₄/MAPbI₃ interface, where the valence and conduction energy level offsets were found to be fixed regardless of changes of E_F in the bandgap. This is further supported by steady-state and time-resolved PL measurements, which clearly exhibit an enhanced PL for MAPbI₃ due to interfacial FRET from PEA₂PbI₄. Our findings provide a solid fundamental understanding of the electronic properties of the prototypical 2D PEA₂PbI₄ perovskite and its interface with 3D MAPbI₃, as well as the interfacial optoelectronic processes. With this, 2D/3D material interface engineering toward more stable and efficient perovskite solar cells can be better harnessed.

4. Experimental Section

Sample Preparation: Substrates with various organic films, including poly(3,4-ethylenedioxythiophene) polystyrene sulfonate (Clevios HIL 1.3, from H. C. Starck Clevios GmbH), PEDOT:PSS (AI 4083 from Heraeus), poly[bis(4-phenyl)(2,5,6-trimethylphenyl)amine] (PTAA from Sigma-Aldrich) and poly(ethyleneimine) (PEIE and PEIE-BuOH from Sigma-Aldrich) were prepared according to our previous method.^[39,40] The PEA₂PbI₄ solution was prepared with 199.27 mg of PEAI (98%, Sigma-Aldrich) and 184.4 mg of PbI₂ (99.999%, Sigma-Aldrich) dissolved in 1 mL of dimethyl sulfoxide (DMSO, Sigma-Aldrich). The PEA₂PbI₄ solution was spin-coated at 4000 rpm for 30 s onto the substrate and annealed at 100 °C for 10 min. The MAPbI₃ film was prepared according to the reference.^[40] To grow the PEA₂PbI₄ on the MAPbI₃ on top, PEAI solutions dissolved in isopropanol with both 1 mg mL⁻¹ (for thin PEA₂PbI₄ film) and 10 mg mL⁻¹ (for thick PEA₂PbI₄ film) concentrations, and were spin-coated onto the as-prepared MAPbI₃ film at 4000 rpm for 30 s, and annealed at 100 °C for 10 min. All the perovskite films were fabricated in the N₂-filled glove box and directly transferred to the vacuum chambers without air exposure.

Direct and Inverse Photoelectron Spectroscopy: UV photoelectron spectroscopy (UPS) and X-ray photoelectron spectroscopy (XPS)

measurements were conducted using a SPECS PHOIBOS 100 hemispherical analyzer and monochromatized helium discharging lamp (21.22 eV) for UPS and standard Mg K α (1253.6 eV, 60 W of anode power) X-ray source for XPS measurements. To obtain the secondary electron cutoff, a sample bias of -10 V was applied.

Inverse photoelectron spectroscopy (IPES) measurement was conducted using a PSP photon detector and electron gun with a BaO cathode. A bandpass filter of 9.5 eV was applied with the isochromat mode. The base pressure of the analysis chamber was maintained below 2.0×10^{-10} mbar.

Steady-State and Time-Resolved Photoluminescence: Photoluminescence (PL) and photoluminescence excitation (PLE) measurements were conducted using an Edinburgh Instruments FLS 980 spectrometer. Samples were measured in a cryostat at room temperature at a pressure below 0.1 mbar. Steady-state PL measurements were performed with a 450 W Xenon arc lamp and time-resolved measurements using a picosecond pulsed diode laser, model EPL-405, with a wavelength of 405 nm and frequency of 200 kHz.

Supporting Information

Supporting Information is available from the Wiley Online Library or from the author.

Acknowledgements

This study was supported by the Deutsche Forschungsgemeinschaft (DFG, German Research Foundation, Project numbers: 182087777-SFB951 and 423749265-SPP2196 "SURPRISE").

Open access funding enabled and organized by Projekt DEAL.

Conflict of Interest

The authors declare no conflict of interest.

Data Availability Statement

The data that support the findings of this study are available from the corresponding author upon reasonable request.

Keywords

2D/3D perovskites, energy level alignment, interfaces, photoelectron spectroscopy, Ruddlesden-Popper phase

Received: August 4, 2022

Revised: October 10, 2022

Published online: November 4, 2022

- [1] NREL, Best Res. Effic. Chart | Photovolt. Res. | NREL, <https://www.nrel.gov/pv/assets/pdfs/best-research-cell-efficiencies-rev220630.pdf> (accessed: June 2022).
- [2] D. Ma, K. Lin, Y. Dong, H. Choubisa, A. H. Proppe, D. Wu, Y. K. Wang, B. Chen, P. Li, J. Z. Fan, F. Yuan, A. Johnston, Y. Liu, Y. Kang, Z. H. Lu, Z. Wei, E. H. Sargent, *Nature* **2021**, 599, 594.
- [3] R. Lin, J. Xu, M. Wei, Y. Wang, Z. Qin, Z. Liu, J. Wu, K. Xiao, B. Chen, S. M. Park, G. Chen, H. R. Atapattu, K. R. Graham, J. Xu, J. Zhu, L. Li, C. Zhang, E. H. Sargent, H. Tan, *Nature* **2022**, 603, 73.

- [4] H. Min, D. Y. Lee, J. Kim, G. Kim, K. S. Lee, J. Kim, M. J. Paik, Y. K. Kim, K. S. Kim, M. G. Kim, T. J. Shin, S. Il Seok, *Nature* **2021**, 598, 444.
- [5] M. Stolterfoht, C. M. Wolff, J. A. Márquez, S. Zhang, C. J. Hages, D. Rothhardt, S. Albrecht, P. L. Burn, P. Meredith, T. Unold, D. Neher, *Nat. Energy* **2018**, 3, 847.
- [6] J. Warby, F. Zu, S. Zeiske, E. Gutierrez-Partida, L. Frohloff, S. Kahmann, K. Frohna, E. Mosconi, E. Radicchi, F. Lang, S. Shah, F. Peña-Camargo, H. Hempel, T. Unold, N. Koch, A. Armin, F. De Angelis, S. D. Stranks, D. Neher, M. Stolterfoht, *Adv. Energy Mater.* **2022**, 12, 2103567.
- [7] I. C. Smith, E. T. Hoke, D. Solis-Ibarra, M. D. McGehee, H. I. Karunadasa, *Angew. Chemie – Int. Ed.* **2014**, 53, 11232.
- [8] L. Pedesseau, D. Saporì, B. Traore, R. Robles, H. H. Fang, M. A. Loi, H. Tsai, W. Nie, J. C. Blancon, A. Neukirch, S. Tretiak, A. D. Mohite, C. Katan, J. Even, M. Kepenekian, A. C. S. *Nano* **2016**, 10, 9776.
- [9] B. Cheng, T. Y. Li, P. Maity, P. C. Wei, D. Nordlund, K. T. Ho, D. H. Lien, C. H. Lin, R. Z. Liang, X. Miao, I. A. Ajia, J. Yin, D. Sokaras, A. Javey, I. S. Roqan, O. F. Mohammed, J. H. He, *Commun. Phys.* **2018**, 80, 7355.
- [10] E. H. Jung, N. J. Jeon, E. Y. Park, C. S. Moon, T. J. Shin, T. Y. Yang, J. H. Noh, J. Seo, *Nature* **2019**, 567, 511.
- [11] H. Tsai, W. Nie, J. C. Blancon, C. C. Stoumpos, R. Asadpour, B. Harutyunyan, A. J. Neukirch, R. Verduzco, J. J. Crochet, S. Tretiak, L. Pedesseau, J. Even, M. A. Alam, G. Gupta, J. Lou, P. M. Ajayan, M. J. Bedzyk, M. G. Kanatzidis, A. D. Mohite, *Nature* **2016**, 536, 312.
- [12] Y. W. Jang, S. Lee, K. M. Yeom, K. Jeong, K. Choi, M. Choi, J. H. Noh, *Nat. Energy* **2021**, 6, 63.
- [13] G. Grancini, C. Roldán-Carmona, I. Zimmermann, E. Mosconi, X. Lee, D. Martineau, S. Narbey, F. Oswald, F. De Angelis, M. Graetzel, M. K. Nazeeruddin, *Nat. Commun.* **2017**, 8, 15684.
- [14] J. C. Blancon, J. Even, C. C. Stoumpos, M. G. Kanatzidis, A. D. Mohite, *Nat. Nanotechnol.* **2020**, 15, 969.
- [15] Q. Jiang, Y. Zhao, X. Zhang, X. Yang, Y. Chen, Z. Chu, Q. Ye, X. Li, Z. Yin, J. You, *Nat. Photonics* **2019**, 13, 460.
- [16] J. C. Blancon, H. Tsai, W. Nie, C. C. Stoumpos, L. Pedesseau, C. Katan, M. Kepenekian, C. M. M. Soe, K. Appavoo, M. Y. Sfeir, S. Tretiak, P. M. Ajayan, M. G. Kanatzidis, J. Even, J. J. Crochet, A. D. Mohite, *Science* **2017**, 355, 1288.
- [17] K. Leng, I. Abdelwahab, I. Verzhbitskiy, M. Telychko, L. Chu, W. Fu, X. Chi, N. Guo, Z. Z. Chen, Z. Z. Chen, C. Zhang, Q. H. Xu, J. Lu, M. Chhowalla, G. Eda, K. P. Loh, *Nat. Mater.* **2018**, 17, 908.
- [18] C. Ma, D. Shen, T. W. Ng, M. F. Lo, C. S. Lee, *Adv. Mater.* **2018**, 30, 1800710.
- [19] R. Yang, R. Li, Y. Cao, Y. Wei, Y. Miao, W. L. Tan, X. Jiao, H. Chen, L. Zhang, Q. Chen, H. Zhang, W. Zou, Y. Wang, M. Yang, C. Yi, N. Wang, F. Gao, C. R. McNeill, T. Qin, J. Wang, W. Huang, *Adv. Mater.* **2018**, 30, 1804771.
- [20] Y. Chen, S. Yu, Y. Sun, Z. Liang, *J. Phys. Chem. Lett.* **2018**, 9, 2627.
- [21] X. Chen, J. Zhang, C. Liu, Q. Lou, K. Zheng, X. Yin, L. Xie, P. Wen, C. Liu, Z. Ge, *ACS Appl Energy Mater* **2021**, 4, 11112.
- [22] A. A. Sutanto, P. Caprioglio, N. Drigo, Y. J. Hofstetter, I. Garcia-Benito, V. I. E. Quelo, D. Neher, M. K. Nazeeruddin, M. Stolterfoht, Y. Vaynzof, G. Grancini, *Chem* **2021**, 7, 1903.
- [23] Y. Liu, R. Lu, J. Zhang, X. Guo, C. Li, *J. Mater. Chem. A* **2021**, 9, 26086.
- [24] X. Jiang, J. Zhang, Y. Liu, Z. Wang, X. Liu, X. Guo, C. Li, *Nano Energy* **2021**, 90, 106521.
- [25] Z. Liu, K. Meng, X. Wang, Z. Qiao, Q. Xu, S. Li, L. Cheng, Z. Li, G. Chen, *Nano Lett.* **2020**, 20, 1296.
- [26] J. W. Lee, Z. Dai, T. H. Han, C. Choi, S. Y. Chang, S. J. Lee, N. De Marco, H. Zhao, P. Sun, Y. Huang, Y. Yang, *Nat. Commun.* **2018**, 9, 3021.
- [27] S. Zhao, M. Qin, H. Wang, J. Xie, F. Xie, J. Chen, X. Lu, K. Yan, J. Xu, *Sol. RRL* **2020**, 4, 2000282.

- [28] H. Zhai, F. Liao, Z. Song, B. Ou, D. Li, D. Xie, H. Sun, L. Xu, C. Cui, Y. Zhao, *ACS Appl. Energy Mater.* **2021**, *4*, 13482.
- [29] V. E. Madhavan, I. Zimmermann, A. A. B. Baloch, A. Manekkathodi, A. Belaidi, N. Tabet, M. K. Nazeeruddin, *ACS Appl. Energy Mater.* **2020**, *3*, 114.
- [30] J. Yang, S. Xiong, J. Song, H. Wu, Y. Zeng, L. Lu, K. Shen, T. Hao, Z. Ma, F. Liu, C. Duan, M. Fahlman, Q. Bao, *Adv. Energy Mater.* **2020**, *10*, 2000687.
- [31] Y. Bai, S. Xiao, C. Hu, T. Zhang, X. Meng, H. Lin, Y. Yang, S. Yang, *Adv. Energy Mater.* **2017**, *7*, 1701038.
- [32] L. Zhu, Q. Lu, C. Li, Y. Wang, *Z. Deng, Chinese Chem. Lett.* **2021**, *32*, 2259.
- [33] F. Zu, P. Amsalem, M. Ralaierisoa, T. Schultz, R. Schlesinger, N. Koch, *ACS Appl. Mater. Interfaces* **2017**, *9*, 41546.
- [34] M. Oehzelt, N. Koch, G. Heimel, *Nat. Commun.* **2014**, *5*, 5174.
- [35] P. Chen, Y. Bai, S. Wang, M. Lyu, J. H. Yun, L. Wang, *Adv. Funct. Mater.* **2018**, *28*, 1706923.
- [36] G. Li, J. Song, J. Wu, Z. Song, X. Wang, W. Sun, L. Fan, J. Lin, M. Huang, Z. Lan, P. Gao, *ACS Energy Lett.* **2021**, *6*, 3614.
- [37] Z. Wang, Q. Lin, F. P. Chmiel, N. Sakai, L. M. Herz, H. J. Snaith, *Nat. Energy* **2017**, *2*, 17135.
- [38] M. Stolterfoht, P. Caprioglio, C. M. Wolff, J. A. Márquez, J. Nordmann, S. Zhang, D. Rothhardt, U. Hörmann, Y. Amir, A. Redinger, L. Kegelmann, F. Zu, S. Albrecht, N. Koch, T. Kirchartz, M. Saliba, T. Unold, D. Neher, *Energy Environ. Sci.* **2019**, *12*, 2778.
- [39] D. Shin, F. Zu, N. Koch, *A. P. L. Mater.* **2021**, *9*, 081104.
- [40] D. Shin, F. Zu, A. V. Cohen, Y. Yi, L. Kronik, N. Koch, *Adv. Mater.* **2021**, *33*, 2100211.
- [41] F. Zu, D. Shin, N. Koch, *Mater. Horiz.* **2022**, *9*, 17.
- [42] P. Schulz, L. L. Whittaker-Brooks, B. A. Macleod, D. C. Olson, Y. L. Loo, A. Kahn, *Adv. Mater. Interfaces* **2015**, *2*, 1400532.
- [43] N. K. Noel, S. N. Habisreutinger, B. Wenger, Y. H. Lin, F. Zhang, J. B. Patel, A. Kahn, M. B. Johnston, H. J. Snaith, *Adv. Energy Mater.* **2020**, *10*, 1903231.
- [44] M. Ralaierisoa, I. Salzmann, F. S. Zu, N. Koch, *Adv. Electron. Mater.* **2018**, *4*, 1800307.
- [45] M. Dyksik, S. Wang, W. Paritmongkol, D. K. Maude, W. A. Tisdale, M. Baranowski, P. Plochocka, *J. Phys. Chem. Lett.* **2021**, *12*, 1638.
- [46] J. Bardeen, *Phys. Rev.* **1947**, *71*, 717.
- [47] S. Braun, W. R. Salaneck, M. Fahlman, *Adv. Mater.* **2009**, *21*, 1450.
- [48] J. P. Yang, F. Bussolotti, S. Kera, N. Ueno, *J. Phys D Appl Phys* **2017**, *50*, 423002.
- [49] S. Kahmann, E. K. Tekelenburg, H. Duim, M. E. Kamminga, M. A. Loi, *Nat. Commun.* **2020**, *11*, 2344.
- [50] J. Yin, R. Naphade, L. Gutiérrez Arzaluz, J. L. Brédas, O. M. Bakr, O. F. Mohammed, *ACS Energy Lett.* **2020**, *5*, 2149.
- [51] F. Zu, M. Roß, L. Frohloff, D. Shin, N. Tessler, S. Albrecht, N. Koch, *Sol. RRL* **2022**, *6*, 26.
- [52] F. Zu, P. Amsalem, D. A. Egger, R. Wang, C. M. Wolff, H. Fang, M. A. Loi, D. Neher, L. Kronik, S. Duhm, N. Koch, *J. Phys. Chem. Lett.* **2019**, *10*, 601.
- [53] J. Endres, D. A. Egger, M. Kulbak, R. A. Kerner, L. Zhao, S. H. Silver, G. Hodes, B. P. Rand, D. Cahen, L. Kronik, A. Kahn, *J. Phys. Chem. Lett.* **2016**, *7*, 2722.
- [54] S. Silver, J. Yin, H. Li, J. L. Brédas, A. Kahn, *Adv. Energy Mater.* **2018**, *8*, 1703468.
- [55] W. Peng, J. Yin, K. T. Ho, O. Ouellette, M. De Bastiani, B. Murali, O. El Tall, C. Shen, X. Miao, J. Pan, E. Alarousu, J. H. He, B. S. Ooi, O. F. Mohammed, E. Sargent, O. M. Bakr, *Nano Lett.* **2017**, *17*, 4759.
- [56] N. Koch, S. Duhm, J. P. Rabe, A. Vollmer, R. L. Johnson, *Phys. Rev. Lett.* **2005**, *95*, 4.
- [57] J. P. Yang, F. Bussolotti, S. Kera, N. Ueno, *J. Phys D Appl Phys* **2017**, *50*, 423002.
- [58] W. Bardyszewski, L. Hedin, *Phys. Scr.* **1985**, *32*, 439.
- [59] W. Meng, K. Zhang, A. Osvet, J. Zhang, W. Gruber, K. Forberich, B. Meyer, W. Heiss, T. Unruh, N. Li, C. J. Brabec, *Joule* **2022**, *6*, 458.
- [60] S. Panuganti, L. V. Besteiro, E. S. Vasileiadou, J. M. Hoffman, A. O. Govorov, S. K. Gray, M. G. Kanatzidis, R. D. Schaller, *J. Am. Chem. Soc.* **2021**, *143*, 4244.
- [61] E. R. Nandayapa, K. Hirslandt, C. Boeffel, E. L. Unger, E. J. W. List-Kratochvil, *Adv. Opt. Mater.* **2021**, *9*, 2001317.
- [62] W. Chi, S. K. Banerjee, *Adv. Funct. Mater.* **2022**, *32*, 2200029.